Topical triple-strategy nanoemulsion formulations of cetrimide for treating methicillin-resistant *Staphylococcus aureus*-infected skin wounds

Rawia Khalil[1], Mohamed F. AbdelHameed[2], Shaymaa A. Ismail[3], Amira A. Hassan[3], Marwa E. Shabana[4], Wenli Zhang[5], and Eman S. Shalaby[1]*

ABSTRACT

Wound management remains a global health concern due to its fatal complications, and cetrimide (CET) is an antimicrobial quaternary ammonium chemical used in wound healing. This study aimed to develop and assess the therapeutic potential of a CET-loaded nanoemulsion for treating methicillin-resistant *Staphylococcus aureus*-infected wounds. A high-speed homogenization method was used for preparing nanoemulsions containing CET, sesame oil, and linalool. Entrapment efficiency, droplet size, and zeta potential were evaluated to identify the optimal formulations. Further characterization included *in vitro* release studies, differential scanning calorimetry (DSC), Fourier-transform infrared spectroscopy (FTIR), and transmission electron microscopy. The selected formulations were subsequently evaluated for their *in vivo* wound healing efficacy in a full-thickness wound model. The formulated nanoemulsion demonstrated high entrapment efficiency (92.71–98.57%), with droplet sizes of 150–399 nm and zeta potential of +10–+27.9 mV, suggesting favorable physical stability. The *in vitro* drug release followed a biphasic pattern. DSC peaks of the drug were diffused in the formulation, suggesting its presence in the amorphous form. FTIR study showed no new peaks, suggesting no chemical interaction between the drug and the formulation components. *In vivo* evaluation of wound healing efficacy revealed a marked reduction in wound size following treatment with selected CET-loaded nanoemulsions. In addition, a significant decrease in tumor necrosis factor-alpha levels, alongside increased expression of B-cell lymphoma 2 and collagen type I, was observed in treated rats. Histological analysis further supported these findings, revealing near-normal tissue architecture. Collectively, these results indicate that CET-loaded nanoemulsions represent a promising approach for enhancing topical wound healing outcomes.

Keywords:
Nanoemulsion; Cetrimide; Wound healing; Methicillin-resistant *Staphylococcus aureus*; Histopathology

***Corresponding author:**
Eman S Shalaby,
es.el-ela@nrc.sci.eg

How to cite this article:
Khalil R, AbdelHameed MF, Ismail SA, *et al.* Topical triple-strategy nanoemulsion formulations of cetrimide for treating methicillin-resistant *Staphylococcus aureus*-infected skin wounds. *Biomater Transl.* **2025**

doi: 10.12336/bmt.25.00039

1. Introduction

Accelerating the wound-healing process remains a challenge for researchers worldwide. The complex process of wound healing involves several interconnected phases, such as homeostasis, inflammation, proliferation, and remodeling.[1] Among the most prevalent bacterial strains found in infected wounds are *Pseudomonas aeruginosa*, *Staphylococcus aureus*, and methicillin-resistant *S. aureus* (MRSA). The wound healing process may be delayed if certain bacteria, such as MRSA, colonize and multiply in the wound tissue.

Semisolid nanoemulsions are pharmaceutical formulations that are administered topically.[2,3] These nanoemulsions can be prepared using high-energy techniques, such as high-shear stirring, high-pressure homogenization, or ultrasound

generation.[4] Semisolid nanoemulsions are generally preferred because their tiny size (between 100 and 600 nm) allows them to deposit evenly on the skin and improves the efficient transport of active substances to the skin.[3,5] Furthermore, semisolid dose forms are more comfortable, easier to apply, and spread more evenly on the skin surface.[6] In essence, the semisolid formulation comprises a variety of medications with distinct therapeutic properties embedded in a suitable semisolid foundation, which may be either hydrophilic or hydrophobic.[3]

Cetrimide (CET), also known as alkyl trimethylammonium bromide, is an antimicrobial quaternary ammonium chemical.[7] As an alternative to chlorhexidine with comparable properties, CET is a cationic surfactant that is effective against both Gram-positive and Gram-negative bacteria and has antifungal properties.[8] It is applied topically as a 0.5% cream in conventional treatments for burns and wounds.[9,10] and is considered completely non-toxic at concentrations of up to 2%.[8] CET is known for its disinfectant and wound healing properties.[11] It readily dissolves in water, dissociating in aqueous solution to produce the cation responsible for CET's antimicrobial action.[12] However, CET has low bioavailability and poor tissue retention due to its hydrophilicity. Therefore, incorporating it in a water-in-oil nanoemulsion offers a promising method for controlled drug release and enhanced deposition into deeper epidermal layers. A commonly used non-ionic surfactant in topical formulations is Tween 80. It is compatible with acidic and basic conditions and is less prone to hydrolysis and degradation by microorganisms. Furthermore, Tween 80 is considered non-toxic, making it safe for topical administration.[13]

Owing to their small size, nanoemulsions can pass through the skin surface, enhancing the penetration of active components.[14] They are made up of tiny droplets of one immiscible liquid scattered inside another and have been extensively utilized for drug delivery via a variety of routes, such as intravenous, oral, and ocular administration. However, only a few studies have explored nanoemulsions as topical carriers, despite their advantages such as high drug-loading capacity and excellent skin penetrability.[15] Among the several ways to deliver nanoemulsions, their topical application has gained popularity due to these benefits. Traditional topical and dermatological formulations often face several challenges, including high microbial resistance,[16] poor skin adhesion, low permeability, and reduced patient compliance. In addition, effective treatment of tissue disorders and wound healing requires the drug to remain at the target site for a sufficient duration.[17] In contrast to conventional formulations, nanoemulsions enable efficient skin deposition, offer thermodynamic stability, and possess a flexible nanostructure conducive for enhanced skin penetration. Furthermore, the spontaneous formation of nanoemulsion systems simplifies industrial production and scalability.[18]

The synthesis of CET-based nanoemulsions has not been the subject of any prior research. The current study used sesame oil or linalool as the oil phase to prepare CET nanoemulsions. The aims were to assess the effectiveness of these CET nanoemulsions against MRSA-infected wounds, evaluate their anti-inflammatory properties, and examine their *ex vivo* skin penetration and deposition capabilities. The formulations were designed to combine selected oils with CET, an antimicrobial medication, to improve patient compliance, enhance drug release, and achieve a synergistic therapeutic effect in the treatment of infected wounds.

2. Materials and methods

2.1. Materials

CET (003100 [CAS 8044-71-1]) was purchased from Pharmalog, Egypt. Span 60 (S7010 [CAS 1338-41-6]), Span 80 (S6760 [CAS 1338-43-8]), and linalool (L2602 [CAS 78-70-6]) were purchased from Sigma-Aldrich, United States (US). Sesame oil was purchased from Nefertari Natural Body Care Line, Egypt. All other chemicals were of reagent or analytical grade and were used without further purification. Distilled water was used in all preparations.

2.2. Animals

The National Research Centre (NRC)'s animal house in Egypt provided 8 weeks old male Wistar albino rats weighing 180–200 g. At a temperature of 23 ± 2°C and a relative humidity of 50 ± 10%, the rats were kept in hygienic cages with 12-h light and dark cycles. They were given a chow meal and unlimited access to tap water. All *in vivo* studies adhered to the guidelines of the National Institutes of Health for Care and Use of Laboratory Animals, Publication No. 8023, amended 1978, and the Animal Research Reporting of *in vivo* Experiments. The study protocol was approved by the NRC's Medical Research Ethics Committee (ethical approval number 0980223).

2.3. Experimental design

2.3.1. Preparation of CET nanoemulsions

Several techniques for generating nanoemulsions, including phase inversion, ultrasonication, and high-pressure homogenization, have been reported.[19,20] In this study, the high-speed homogenization method described by Samadi *et al.*,[21] with modifications, was employed to synthesize CET, sesame oil, and linalool nanoemulsions. At room temperature, an aqueous phase containing CET and Cremophore RH 40 (07076 [CAS 61788-85-0], Sigma Aldrich, USA) was magnetically agitated until it was completely dissolved. An oil phase comprising the oils (linalool or sesame oil) and the mixture of oil-soluble surfactants (Span 60 and Span 80) was heated to 40°C until it completely melted. Following the addition of the aqueous phase to the oil phase, the mixture

[1]Department of Pharmaceutical Technology, Pharmaceutical and Drug Research Institute, National Research Centre, Giza, Egypt; [2]Department of Pharmacology, Medical Research and Clinical Studies Institute, National Research Centre, Giza, Egypt; [3]Department of Chemistry of Natural and Microbial Products, Pharmaceutical and Drug Industries Research Institute, National Research Centre, Giza, Egypt; [4]Department of Pathology, Medical Research and Clinical Studies Institute, National Research Centre, Giza, Egypt; [5]Department of Pharmaceutics, School of Pharmacy, China Pharmaceutical University, Nanjing, Jiangsu, China

was homogenized for 5 min at 20,000 rpm and then stirred for 20 min at 600 rpm using a magnetic stirrer.

2.3.2. Encapsulation efficiency

To determine the amount of the drug entrapped in the lipidic nanoparticles, 1 g of the prepared formulation was transferred into tubes containing 10 mL of water and centrifuged at 7000 rpm for 1 h using a Union 32R centrifuge (Hanil Scientific Inc., Korea). The resulting supernatant was filtered through a 0.2 μm Millipore syringe filter, appropriately diluted, and analyzed using a ultraviolet spectrophotometer (2401/PC, Shimadzu Corporation, Japan) at 209 nm against blanks. The concentration of free drug in the supernatant was used to calculate the encapsulation efficiency. All experiments were performed in triplicate.[22,23] The formula for encapsulation efficiency calculation is as follows:

EE (%) = (total amount of drug encapsulated/total amount of drug added) * 100 (I)

2.3.3. Particle size, polydispersity index (PDI), and zeta potential measurements

Using a Zetasizer (Nano Series ZS90, Malvern Instruments, Ltd., United Kingdom), dynamic light scattering was employed to characterize the particle size, PDI, and zeta potential. The dispersion was diluted with distilled water (1:1000 v/v) prior to measurement, followed by short-term bath sonication.[22,23] The size distribution of the prepared nanoemulsions was described via the PDI, which reflects the uniformity of the particle size. All measurements were recorded in duplicate.

2.3.4. In vitro drug release

The dialysis bag diffusion method was employed to investigate the *in vitro* release of CET from the optimized nanoemulsion using cellulose membrane dialysis tubing (molecular weight cut-off 12,000–14,000 g/mol; D 9277, Sigma-Aldrich, US). To prevent leakage, 1 g of the formulation—equal to 5 mg of CET—was placed inside a dialysis bag and sealed on both sides. To preserve sink conditions, the bags were subsequently placed in amber-colored, wide-mouthed glass bottles with 100 mL (10% v/v) of ethanolic phosphate buffer (pH 5.5). The study was conducted at 32 ± 0.5°C in a thermostatic shaking water bath (SV 1422, Memmert, Germany)[22,24] and then centrifuged at 100 rpm for 24 h. At 1, 2, 3, 4, 5, 6, and 24 h time points, 5 mL aliquots of the release medium were collected and replenished with fresh medium. The concentrations of CET in the samples were assessed spectrophotometrically and compared with blanks at 209 nm[25] via the regression equation of a calibration curve constructed in the release medium. For comparison, the release profile of a plain CET solution containing the same quantity of the drug in the release medium was examined. The ratio of the amount of CET released to the initial amount of CET in the dialysis bag was used to calculate the cumulative release percentage. All tests were performed in triplicate.

To study the release mechanism of CET from the optimized nanoemulsion, a kinetics study of the release data was conducted. The data were fitted to three different mathematical models: the Higuchi model (% cumulative drug released vs. square root of time), the zero-order model (% cumulative drug released vs. time), and the first-order model (log% cumulative drug retained vs. time).

2.3.5. Fourier-transform infrared spectroscopy (FT-IR)

A FT-IR spectrophotometer (FT/IR 6100, Jasco, Japan) was used to determine the chemical integrity and potential chemical interactions among the ingredients. In contrast to the liquid samples (Span 80, Span 85, linalool, sesame oil, and Cremophore RH 40), the solid samples of the drug (CET) and the freeze-dried formulations were combined separately with potassium bromide and compressed under hydraulic pressure of 200 kg/cm^2 for 2 min to produce compact disks. Every sample was scanned on a blank KBr pellet backdrop at frequencies between 4,000 and 400 cm^{-1}.[26,27]

2.3.6. Differential scanning calorimetry (DSC)

A differential scanning calorimeter (DSC; DSC-60, Shimadzu Corporation, Japan) was used to analyze 2 mg CET samples, the employed single components, and specific freeze-dried nanoemulsions to ascertain their thermal properties. The sample was heated from 25°C to 300°C and then cooled at a rate of 10°C/min before DSC scans were performed. After being recorded, the thermograms were examined for incompatibility, such as notable changes or the emergence of new peaks.[28,29]

2.3.7. Transmission electron microscopy

The morphologies of the selected nanoformulations were examined via transmission electron microscopy (JEM-1230, JEOL Ltd., Japan) at an accelerating voltage of 80 kV. One drop of the diluted sample was applied to copper grids for examination after being stained with 2% (w/v) phosphotungstic acid for 30 s.

2.3.8. Antimicrobial efficacy

Using the well-diffusion method, the antibacterial activity of the selected CET formulations was investigated against MRSA ATCC 33591 and *S. aureus* ATCC 6538.[30] Initially, nutrient agar plates were evenly covered with 200 μL of each nutrient broth cell suspension, matching a 0.5 McFarland standard solution. Next, 7 mm-diameter wells were created in the agar plates, and 100 μL of each sample dissolved in dimethyl sulfoxide was added to each well. The wells were then incubated for 24 h at 37°C. The experiment was conducted in duplicate, with the average inhibitory zone diameter measured in millimeters. In addition, by examining several concentrations in distinct wells, the minimum inhibitory concentration (MIC), or the least growth-preventable concentration, of each sample was estimated.

2.3.9. In vivo model for the induction of MRSA infection in wounds

The rats were placed under anesthesia, and a 1.5 × 1.5 cm incision was made between their shoulders. The wound became infected within 24 h after 0.1 mL of a mixture containing MRSA (1 × 10^9 colony-forming units) was administered. Each of the five groups—group 1 being the negative control, group 2 being the positive control treated with Fucidin, group 3 being the CET-free solution, and groups 4 and 5 being the selected CET

formulations—was assigned at random once the wound was created. Starting 24 h after the initial procedure and continuing for 10 days afterward, the formulations were applied topically to the wound region once daily. Each rat was checked for signs of infection and any fluid coming from the wounds.

2.3.10. Wound healing assessment

The progressive change in the wound area was evaluated on days 3, 7, and 10, and the wound contraction percentage was subsequently calculated.

(a) Wound size

Wound healing progress was estimated by determining the decrease in wound size with time.[31] To visually assess the wound incisions, the Samsung Galaxy M34 smartphone (Korea), which has a triple-camera system with 50-megapixel, 8-megapixel, and 2-megapixel sensors, was used to take photos of the wounds. The images were then downloaded to a computer running the ImageJ application (http://rsbweb.nih.gov/ij/download.html). The wound area was measured on days 0, 3, 7, and 10, and the equation to compute the wound contraction percentage is as follows:[32]

$$\text{Wound contraction (\%)} = (A0\text{-}An/A0) * 100 \quad \text{(II)}$$

where *n* is the day when the measurement was performed, A0 is the area of wound zero day post injury, An the area of wound when the measurement performed

(b) Biochemical analysis

On the 10th day after the injury, the rats were sacrificed via anesthesia and cervical dislocation. The injured tissues were removed. A 20% (w/v) homogenate was prepared in ice-cooled saline (0.9% sodium chloride) through a homogenizer (MPW-120, Medical Instruments, Poland). The mixture was then centrifuged for 6 min at 4°C and 4000 rpm (2k15, Sigma Laborzentrifugen GmbH, Germany).[33] The supernatants were collected to estimate the contents of B-cell lymphoma 2 (BCL2), tumor necrosis factor-alpha (TNF-α), and collagen type I (Col-I) using enzyme-linked immunosorbent assay (ELISA) kits (SunLong Biotec Co., Ltd., China).[24,34] Analyses were performed in compliance with the manufacturer's instructions.

(c) Histological examination

Rats from each treatment group were anaethesized at the end of the 10-day treatment period, and the injured skin sections were processed for histological examination. A microtome was used to cut serial 4 μm-thick sections of the wounds after they had been immersed in paraffin and preserved in 10% formalin for 24 h. Using a light electric microscope (CX41, Olympus, Japan), the slices were placed on glass slides, deparaffinized, and stained with hematoxylin–eosin for histological analysis.

Keratinization, which has a major influence on the wound healing process, was assessed via a semiquantitative scoring approach. The re-epithelialization process of the epidermis was assessed using the wound scoring scale, as explained by Gal *et al.*[35] (**Table 1**).

2.3.11. Statistical analysis

One-way analysis of variance (ANOVA) was used for all quantitative comparisons in the study, and Tukey's multiple comparison *post hoc* test was used (Prism 8.0, GraphPad, US). A $p<0.05$ was considered as statistically significant. All data are presented as mean ± standard error of the mean.

3. Results and discussion

3.1. Preparation and selection of components

There were no observed indications of coalescence or separation in any of the six formulations made using the various combinations listed in **Table 2**. The generation of nanoemulsions had previously been accomplished using a high-pressure homogenizer.[36] By comparing a constant ratio of oil with various mixing ratios, the optimal combination was identified. Furthermore, another critical factor was the choice of surfactant.[37] Surfactants facilitated the dispersion process by lowering the interfacial tension and producing a flexible film that could easily bend around the droplets. In addition, the presence of cosurfactants enhanced the flexibility of the interfacial film, allowing it to adapt to the unique curvatures required to stabilize the nanoemulsion across a wide variety of compositions.[38] Cremophore RH40 was used as a cosurfactant, and Span 80 and Span 60 were used as surfactants. Sorbitan esters, often known as Tweens or Spans, are non-ionic surfactants commonly used in drug delivery systems due to their low toxicity, non-irritant nature, and ability to facilitate the formation of various nanocarriers. The lipophilic liquid emulsifying agent, Span 80, has a propensity to create water-in-oil emulsions,[19] and Span 60 was previously reported in formulations of nanoemulsions.[39] Given that the surface charges of CET are essential for its antibacterial activity, non-ionic surfactants (Span 80 and Span 60) were used in this work without attempting to alter them. In addition, a decrease in the internal phase-to-interfacial film volume ratio reflects the formation of a thicker surfactant film, particularly

Table 1. Wound scoring scales for semiquantitative evaluation of histological skin samples based on the re-epithelialization process

Scale	Re-epithelialization
0	Only the thickness of the cut edges
1	Migration of cells <50%
2	Migration of cells ≥50%
3	Bridged the excision
4	Keratinization

Table 2. Composition of cetrimide nanoemulsions

Formulations/ingredients	F1	F2	F3	F4	F5	F6
Sesame oil (mL)	1.4	1.4	1.4	-	-	-
Linalool (mL)	-	-	-	1.4	1.4	1.4
Cremophore RH 40 (mL)	0.2	0.2	0.2	0.2	0.2	0.2
H_2O (mL)	2.4	2.4	2.4	2.4	2.4	2.4
Span 60 (g)	3.6	3.0	2.4	3.6	3.0	2.4
Span 80 (mL)	2.4	3.0	3.6	2.4	3.0	3.6
Cetrimide (mg)	50	50	50	50	50	50

when polymeric cosurfactants, such as Cremophore RH 40, are applied. This suggests enhanced stability and a potential barrier to drug delivery, as previously reported.[40]

In this study, the oil phase consisted of linalool or sesame oil. Linalool, a monoterpene alcohol with weak water solubility, is commonly found in essential oils from plants such as coriander and is known for its potent antibacterial and wound-healing properties.[41,42] Sesame oil comprises approximately 41% linoleic acid and is rich in antioxidant compounds, such as tocopherols and phenolic compounds.[43] It also exhibits potent antimicrobial properties.[44]

3.2. Encapsulation efficiency

Table 3 presents the computed encapsulation efficiencies of the produced nanoemulsions. The drug was successfully encapsulated by all of the produced nanoemulsions, with EE percentages ranging from 92.71% to 98.57%. The high water solubility of CET in the hydrophilic phase of the produced nanoemulsion may be the reason for the high encapsulation effectiveness. Notably, comparable outcomes were reported for several hydrophilic medications.[45-47]

3.3. Particle size, zeta potential, and PDI measurement

Table 3 shows the particle size, zeta potential, and PDI values. The formulations were suitable for topical application, as their average particle size fell within the nanoscale range (150.8–399.01 nm). Comparable ranges of particle sizes were reported by Liao *et al.*[48] and Hidajat *et al.*[49] It has been reported that a particle size lower than 400 nm is favorable for topical delivery.[22] Meanwhile, the nano-system containing sesame oil had a smaller particle size, a result aligning with previous studies.[50] The positive charge of the zeta potential, ranging from +10.8 mV to +27.2 mV, could be attributed to the positive charge of the drug. The surface charge of CET was preserved in the formulations, which is important because the antibacterial action of CET depends on its positive charge. Positively charged molecules are more likely to adhere to bacterial surfaces and penetrate the negatively charged bacterial cell membranes.[12] In addition, nanoparticles with surface charges are more stably dispersed due to electrostatic repulsion.[51] The uniformity of particle size distribution is represented by the PDI. PDI values higher than 0.7 indicate a broad and undesirable size distribution in emulsions. In this study, all measured PDI values were <0.7 (**Table 3**), suggesting that the droplet population is homogeneous across all formulations and has little propensity to aggregate.[52]

3.4. *In vitro* release study

The development of regulated drug release methods with broad applicability requires an understanding of the release mechanism and kinetics of a carrier system.[22] **Figure 1** illustrates the release profiles of CET from the investigated water-in-oil nanoemulsion and from its solution. As anticipated, the free CET solution resulted in a slower and lower release after 24 h (13.34%) compared to other formulations with substantially faster release (87.5–100%). This was attributed to the small, globular size of the nanoemulsions and, which results in a larger surface area, and consequently, a faster rate of drug release.[53,54] This suggests that CET is efficiently solubilized in the nano-systems. The PDI value of F3 was lower (0.375) than that of F6 (0.607), indicating that F3 displays greater drug release than F6. As a result, the surface area for drug release was larger in the case of F3. Similar outcomes were reported in previous studies.[53]

Table 3. Encapsulation efficiencies, particle sizes, zeta potentials, and polydispersity indices (PDI) of the prepared nanoemulsions

Formulation	Encapsulation efficiency (%)	Particle size (nm)	Zeta potential (mV)	PDI
F1	98.28±1.34	300±3.47	+10.8±9.41	0.699
F2	92.71±2.89	336±2.82	+20.2±7.32	0.634
F3*	98.36±1.16	150±1.54	+27.2±5.92	0.375
F4	98.82±3.24	399±3.39	+23.2±5.90	0.678
F5	98.02±5.64	378±4.67	+25.3±6.24	0.611
F6*	98.58±2.87	168±5.66	+26.8±6.28	0.607

Note: *indicate that it is the formulation of choice.

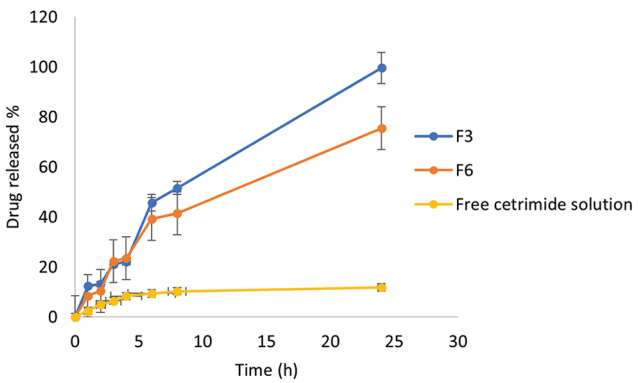

Figure 1. *In vitro* release profiles of the nanoemulsions F3 and F6, as well as that of the free cetrimide solution. Data are expressed as mean ± standard error of the mean.

Table 4 presents the release kinetics analysis of CET from the selected F3 and F6 nanoformulations. According to the data, these nanoemulsions fit the Higuchi model better than the other mathematical models, as shown by the higher correlation coefficient values (R^2 = 0.9845–0.9863). Notably, there have been prior reports of comparable release kinetics for topical nanoemulsions.[18,55] Likewise, the "n" values of more than 0.4 confirmed the non-Fickian diffusion (anomalous) mechanism of CET from the F3 and F6 nanoformulations. Similar reports have also been described previously.[56]

3.5. FT-IR spectrum

The F3 and F6 nanoemulsion systems and their components were analyzed via FTIR, and the resulting spectra are shown in **Figure 2**. Span 60 and Span 80 were the two primary ingredients in the formulations. In the Span 60 spectrum, characteristic peaks were observed at 1690 cm^{-1}, attributed to strong C=O ester bonds, and at 3387 cm^{-1}, corresponding to hydroxyl groups. In formulations F3 and F6, slight shifts in peak positions and reductions in the intensities of the typical peaks for Span 60 were observed. In addition to the peaks at

Table 4. Correlation coefficients of F3 and F6 cetrimide nanoemulsions' release profiles

Formulation	Zero order	First order	Second order	Third order	Higuchi model	Hixson-Crowell model	Korsmeyer-Peppas model	
				R^2			R^2	n
F3	0.9665	0.8258	0.6127	0.4477	0.9845	0.8426	0.9422	0.73
F6	0.9442	0.7412	0.4776	0.3217	0.9863	0.7687	0.9485	0.74

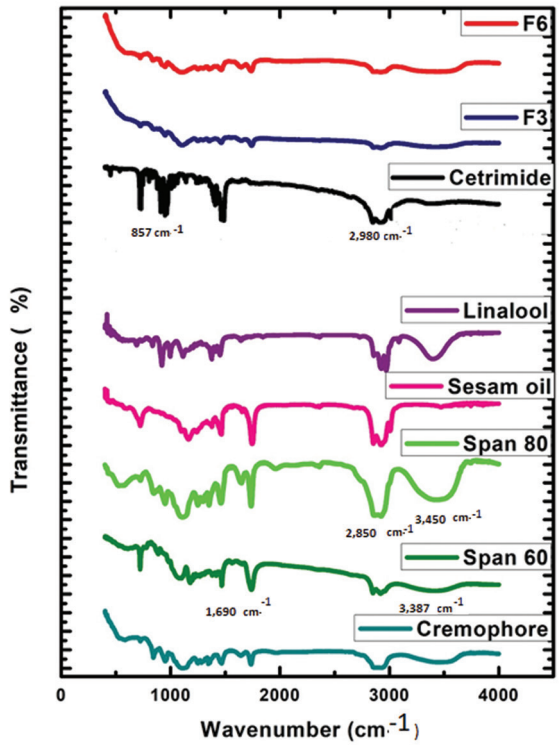

Figure 2. Fourier-transform infrared spectra of the selected formulations and their components

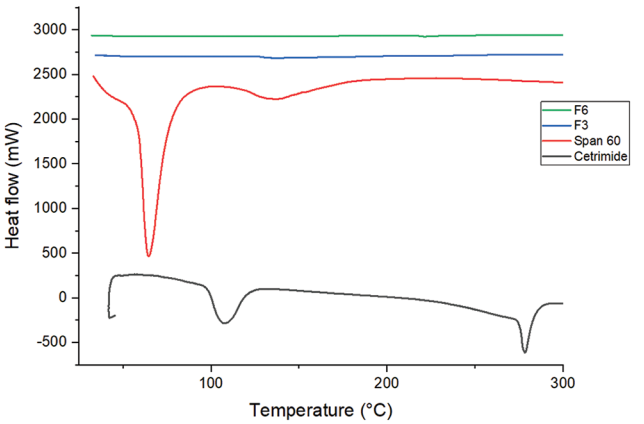

Figure 3. Differential scanning calorimetry thermograms of cetrimide, Span 60, F3, and F6 formulations

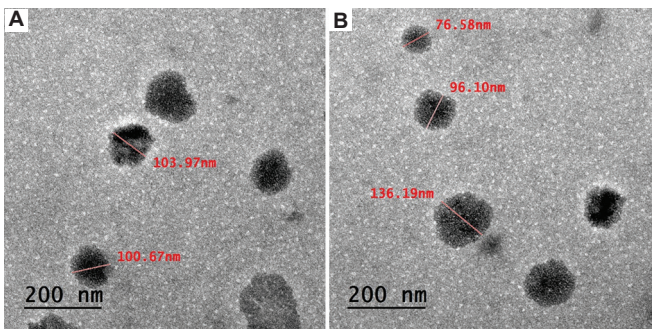

Figure 4. Transmission electron microscopy images of the nanoemulsions (A) F3 and (B) F6. Scale bars: 200 nm; magnification: 50×.

2850 cm^{-1} and 3,450 cm^{-1}, the spectrum of Span 80 showed peaks between 1000 and 2000 cm^{-1}, indicating the presence of stretched hydrogen-bonded O-H. A similar spectrum of span was documented.[57] In addition, the intensities of the peaks of Span 80 were weakened in formulations F3 and F6, indicating successful formation of nanoemulsions.

The distinctive peaks of CET, corresponding to C-H stretching, emerged at 2890 cm^{-1} and 857 cm^{-1}. Sharp bands in the peak at 1400–1500 cm^{-1} were attributed to molecular deformation and the presence of C=C and C=O vibrations in CET. Following incorporation into formulations F3 and F6, the characteristic peaks of CET were diffused, indicating successful encapsulation of the drug within the nanoemulsions. Notably, no additional peaks were observed, indicating that there are no chemical interactions between CET and other substances, thereby implying that the drug remained intact and retained its therapeutic potential. These findings concurred with earlier FTIR research that revealed no interactions between drugs and other excipients.[58]

3.6. Differential scanning colorimetry

Figure 3 shows the thermograms of pure CET, Span 60, and lyophilized F3 and F6 CET-loaded nanoformulations. The DSC thermogram of pure CET exhibited melting endotherms at 107°C and 287°C, corresponding to its melting point.[59] Similarly, Span 60 showed an endothermic peak at 65°C, corresponding to its melting temperature.[60] In contrast, the endothermic peak of CET disappeared in the F3 and F6 formulations, suggesting homogeneous dispersion of the drug throughout the formulation in an amorphous form.[60]

3.7. Transmission electron microscopy

Transmission electron microscopy micrographs of the F3 and F6 formulations are displayed in **Figure 4**. The nanoemulsion droplets were well defined and nearly spherical. They all exhibited a distinct smooth surface.

3.8. *In vitro* antibacterial activity

At concentrations approximately half that of the free drug, the F3 and F6 nanoformulations demonstrated antibacterial activity against the tested strains of *S. aureus* and MRSA. No activity was detected for the blank formula, and the F3 inhibition zone was marginally larger than that of F6 (**Figure 5** and **Table 5**). This result could be attributed to the smaller globular size and

faster rate of drug release. Moreover, the estimated MICs for both F3 and F6 formulations were identical, which were 39 and 156 μg/mL for *S. aureus* ATCC 6538 and MRSA ATCC 33591, respectively (**Table 6**).

3.9. *In vivo* studies of CET nanoformulations

3.9.1. Preliminary study

After 24 h of infection, the MRSA-infected wounds were first compared with the uninfected wounds. According to visual inspection of the MRSA-infected tissues, a superficial swelling hump appeared when the borders of the incision separated from the surrounding healthy tissue, forming a "pocket" beneath the wound surface (**Figure 6**). According to a histopathological analysis, the infected damaged skin had dermal edema beneath an epidermal lining defect. Furthermore, the wound space was filled with a highly inflammatory infiltrate that was typified by widespread neutrophilic infiltration, indicating the significant deterioration effect of MRSA infection on skin wounds. On the other hand, the uninfected wounds presented shallow ulcerative lesions with minimal epidermal and dermal inflammatory reactions and hyalinosis.

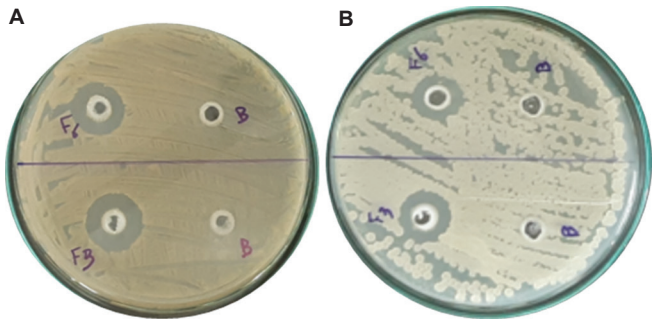

Figure 5. Antibacterial activity of F3 and F6 formulations as well as their free-drug blanks (label B on the petri dish) against (A) *Staphylococcus aureus* ATCC 6538 and (B) methicillin-resistant *S. aureus* ATCC 33591

Infected wounds typically exhibit a distinct microenvironment that hinders wound healing, including high levels of reactive oxygen species, significant inflammation, and compromised immune cells. Therefore, adopting an optimal approach that not only combats bacterial infections but also encourages effective wound healing has attracted research attention.[61,62]

3.9.2. Effects on skin contraction

The efficacy of the prepared nanoformulations was examined via comparisons with other experimental treatment groups, in which the rate of wound contraction was estimated on

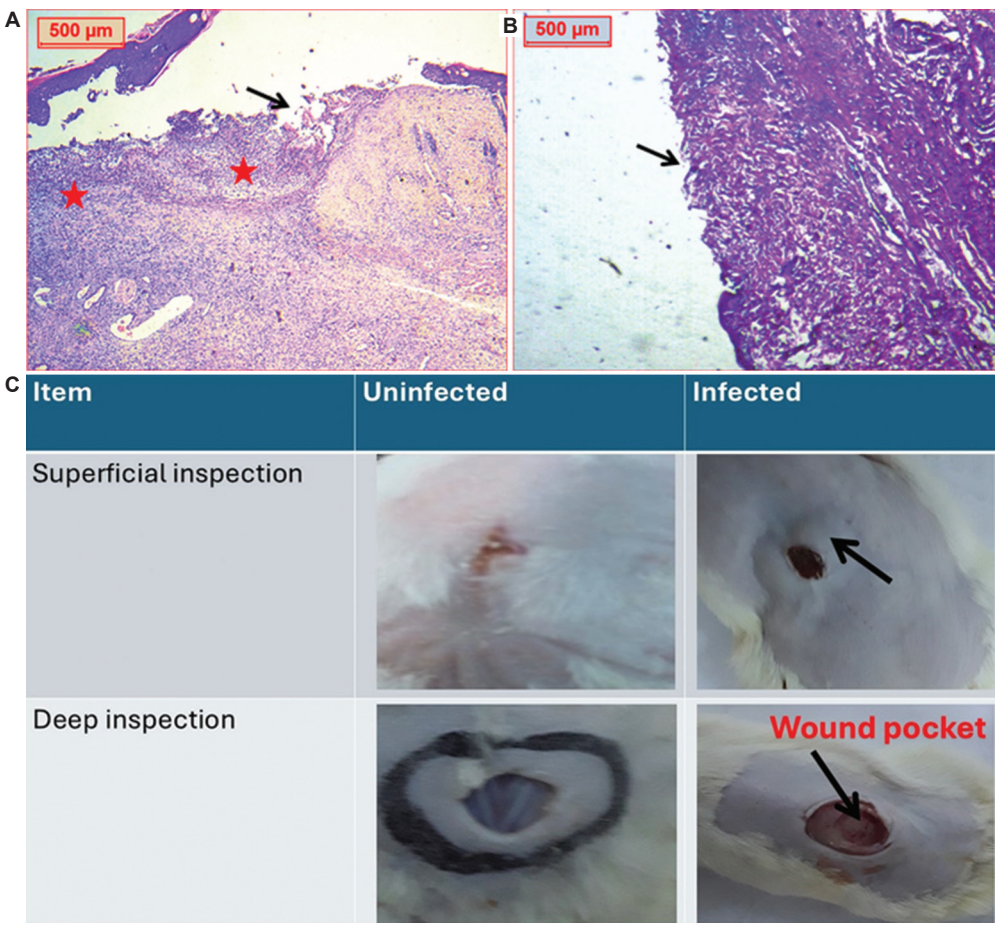

Figure 6. Histopathology and morphology of the wounds. (A) Histopathological examination of the infected wound group showed a disrupted epidermal lining, marked dermal edema, and a dense inflammatory infiltrate occupying the wound gap, predominantly composed of neutrophils. (B) Histopathological examination of the uninfected wound group showed a shallow ulcerative lesion with minimal inflammatory reaction in both the epidermis and dermis, accompanied by areas of hyalinosis. (C) Photographs of the back of rats showing infected and uninfected wounds. Scale bars for A and B: 500 μm; magnification for A and B: 40×.

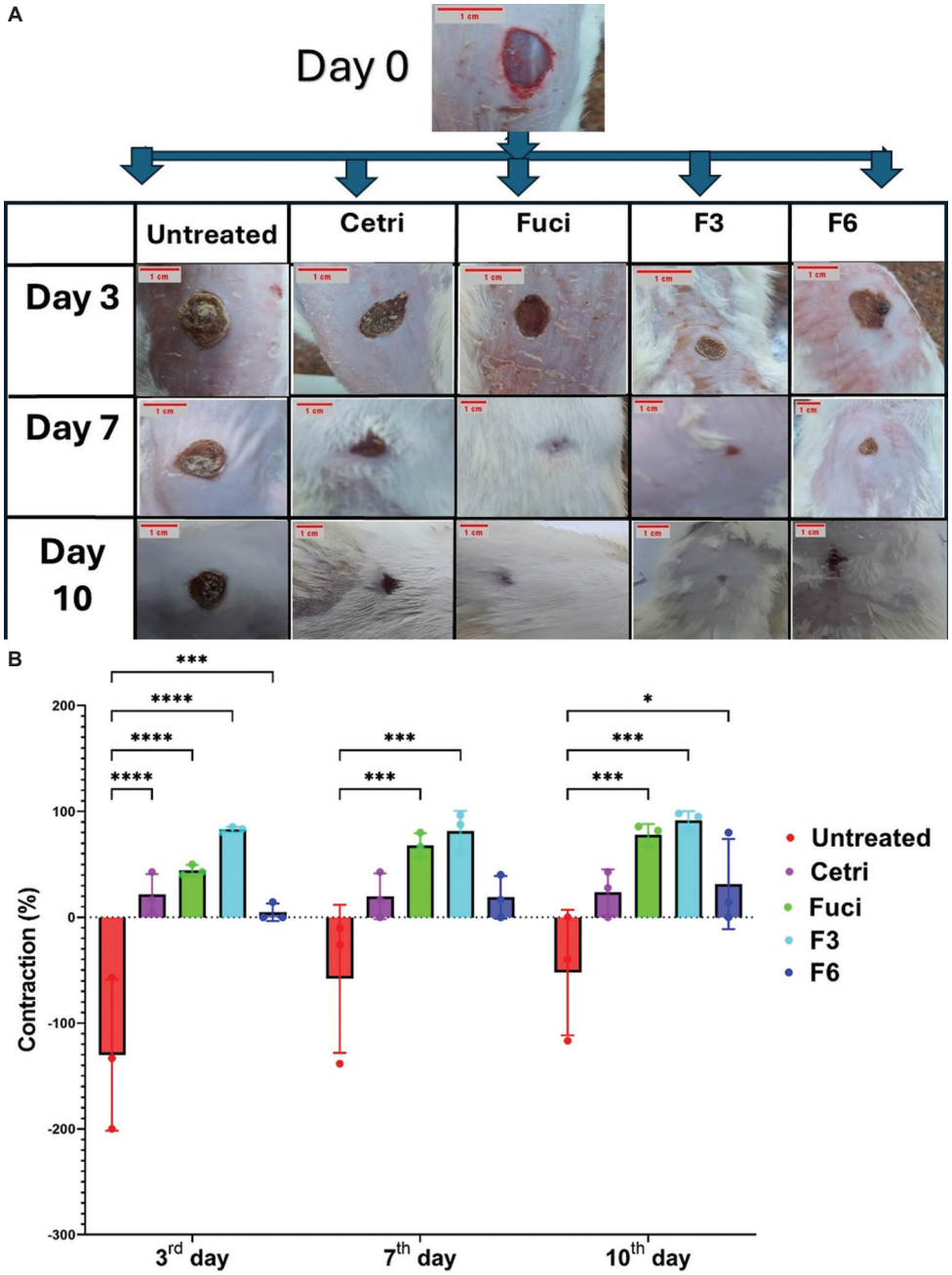

Figure 7. The wound healing activity of the different treatment groups. (A) Rat skin's photographs under different treatment conditions. (B) The contraction percentages across several days.
Notes: *p<0.05, ***p<0.001, ****p<0.0001
Abbreviations: Cetri: Cetrimide, Fuci: Fucidin.

Table 5. *In vitro* antibacterial activity

Sample	Zone of inhibition diameter (mm)	
	Staphylococcus aureus ATCC 6538	Methicillin-resistant *S. aureus* ATCC 33591
Free drug (10 mg/mL)	22	20
F3 (5 mg/mL)	22	20
F3 drug-free formula	-	-
F6 (5 mg/mL)	20	18
F6 drug-free formula	-	-
DMSO	-	-

Abbreviation: DMSO: Dimethyl sulfoxide.

Table 6. MIC values

Formulation	Concentration (μg/mL)	
	Staphylococcus aureus ATCC 6538	Methicillin-resistant *S. aureus* ATCC 33591
F3	39	156
F6	39	156

days 3, 7, and 10, and the results are presented in **Figure 7**. Compared with the free drug and F6 formulation groups, the F3-treated group demonstrated significant improvement in wound contraction, as did the positive control group, with

contraction rates of 82.9% on day 3, 81.4% on day 7, and 91.7% at the end of the treatment period. The high rates of wound contraction and epithelization at the wound site may be attributed to the sustained release ability of the drug.[63] The negative values of wound contraction in infected wounds could be due to the deleterious effect of MRSA bacteria on the wound.

3.9.3. Effects on cellular regulation and tissue homeostasis

Rats subjected to an infected wound model presented elevated levels of TNF-α, which were significantly decreased in the experimental treatment groups. Compared with those in the untreated group, the levels of TNF-α in the Fucidin-treated group were reduced by 60.8%, whereas the free drug-treated group exhibited only 29.4%. Moreover, a significant decrease was observed in the CET nanoformulations with 78.3% and 70.6% reduction in the F3 and F6 treated groups, respectively (**Figure 8**). The expression of anti-inflammatory cytokines should increase, and that of proinflammatory cytokines should decrease during the healing process.[64] For lesioned tissue to be repaired properly, the inflammatory stage of the healing process is critical. Inflammatory mediators, such as cytokines, chemokines, reactive oxygen species, and proteolytic enzymes, are released by inflammatory cells, including neutrophils and activated macrophages. TNF-α is a proinflammatory cytokine that is expressed in higher quantities during the inflammatory phase of the cicatricial process of lesions than at normal levels. The results of the present study indicate that in the infected wounds, TNF-α levels were higher than those in the normal control group. This result was in line with a previous study.[65] Furthermore, the current study revealed that nano-CET could significantly decrease the levels of TNF-α, revealing its potent anti-inflammatory properties. The findings are in agreement with those of a previous study, confirming that nano-CET possesses anti-inflammatory activities by downregulating the levels of TNF-α.[66]

Collagen, a key component of the extracellular matrix, plays an essential role in the management of wound healing. Col-I is known to strongly promote angiogenesis both *in vitro* and *in vivo* via binding to specific integrin receptors. In particular, the C-propeptide fragments of Col-I recruit endothelial cells, initiating angiogenesis in areas involved in healing.[67,68] In the present study, the levels of Col-I were determined. In the untreated group, the levels of Col-I were significantly increased in all treated groups. The CET-free formulation increased the level of Col-I by 134.3% in comparison with that in the untreated group, whereas the nanoformulations improved collagen I levels by 240% and 167% in the F3 and F6 treated groups, respectively (**Figure 9**).

In addition, BCL2 family proteins regulate cell migration, necessary for tissue repair and wound healing. Inhibition may disrupt tissue repair processes, causing wound closure to be delayed or ineffective.[69] In the present study, both the free drug and its nanoformulations increased the level of BCL2, with the highest concentration observed in the F3-treated group, with a 5.5-fold increase in BCL2 levels (**Figure 10**). The enhanced

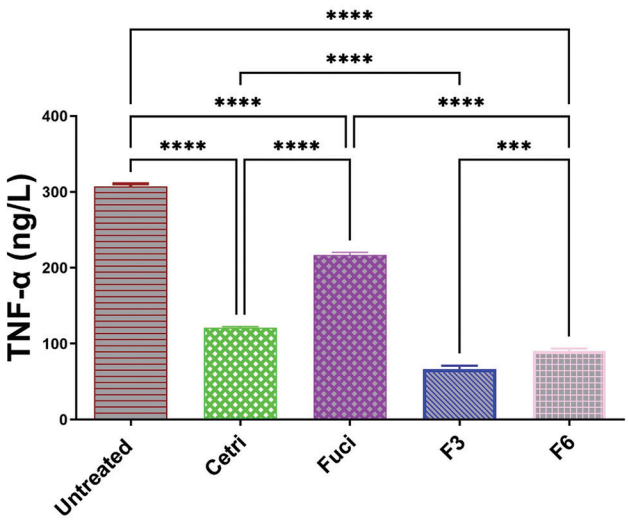

Figure 8. Tumor necrosis factor-alpha (TNF-α) levels across treatment groups.
Notes: ***p<0.001, ****p<0.0001
Abbreviations: Cetri: Cetrimide, Fuci: Fucidin.

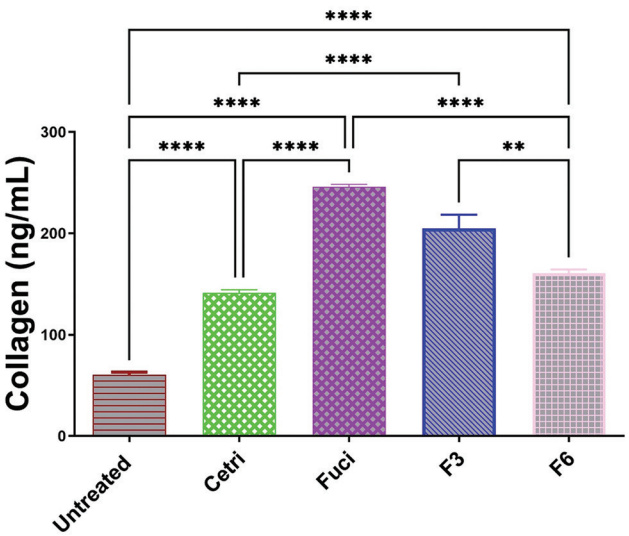

Figure 9. Collagen levels across treatment groups.
Notes: **p<0.01, ****p<0.0001
Abbreviations: Cetri: Cetrimide, Fuci: Fucidin.

efficacy of F3 over F6 could be due to the presence of sesame oil, which has been reported to exhibit a wound healing effect.[70,71]

3.9.4. Histological examination

Through the histological examination of hematoxylin and eosin-stained sections of treated wounded skin, the maturity of the repaired tissues was examined. Different treatments resulted in different responses, as shown in **Figure 11**. Skin sections treated with CET presented a decrease in inflammatory cell levels and the presence of regeneration edges, corresponding to a score of 0. The group treated with Fucidin presented a clean wound devoid of inflammatory cells, though with epidermal loss, and was assigned a score of 1. In contrast, skin sections from the F3-treated group showed marked wound healing, characterized by complete resolution of inflammation, absence of granulation tissue, and epidermal

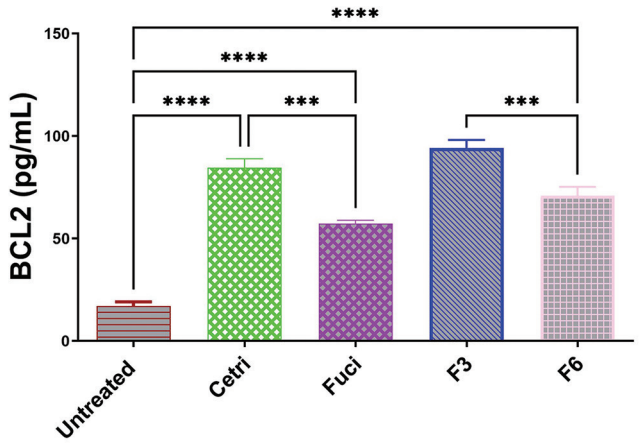

Figure 10. B-cell lymphoma 2 (BCL2) levels across treatment groups. Notes: ***p<0.001, ****p<0.0001.
Abbreviations: Cetri: Cetrimide, Fuci: Fucidin.

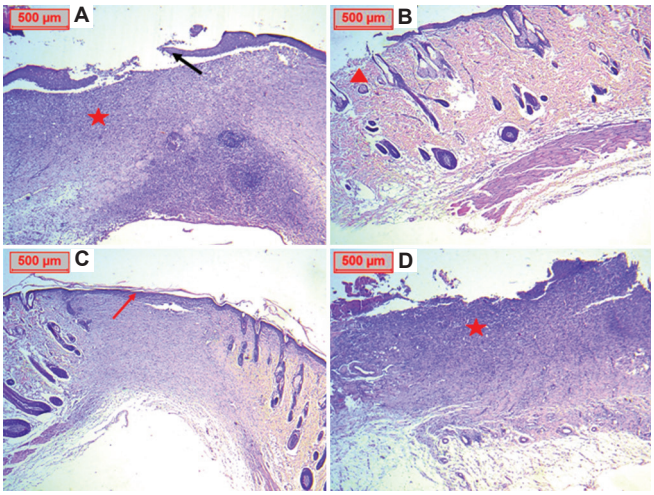

Figure 11. Histopathological photomicrograph of rat skin sections showing: (A) cetrimide-treated group, (B) Fucidin-treated group, (C) F3-treated group, and (D) F6-treated group. Notes: Red star indicates inflammation; red arrowhead indicates clean dermis; black arrow indicates regeneration edge; red arrow indicates re-epithelization. Scale bars: 500 µm; magnifications: 40×.

re-epithelialization, receiving a score of 3. Meanwhile, the group treated with F6 presented skin wounds with marked inflammation, and was given a score of 0.

4. Conclusions

The therapeutic potential of CET and its nanoformulations in the management of MRSA-infected wounds was demonstrated in this investigation. The skin targeting ability and bioavailability of CET were improved by its nanoformulations, enabling more efficient therapeutic delivery. The *in vitro* release profiles of the optimal formulations were all biphasic. *In vivo* research demonstrated the advantages of F3 and F6 formulations in the treatment of full-thickness wounds in rats, as demonstrated by histological analysis, biochemical assays, and wound morphology. This research unequivocally supported nanoemulsions as a novel topical drug delivery method for CET to promote wound healing in skin wounds infected with MRSA.

Nevertheless, experimental design limitations remain in this study. First, the *in vitro* release study used phosphate-buffered solution as the release medium, which does not accurately mimic the complex composition of wound exudate. Additionally, the study was limited to short-term observations (7–14 days), potentially overlooking delayed relapse. The use of rats may not fully replicate the dynamics of human wound healing. Moreover, the absence of immunocompromised models is a critical limitation, especially considering the relevance of such models for studying chronic MRSA-infected wounds. Another important consideration is the lack of long-term safety evaluation for the nanoparticle emulsion, especially concerning its potential impact on skin barrier integrity with prolonged use. Future investigations should prioritize chronic exposure studies and barrier function assays to ensure the safety of repeated applications. Furthermore, while TNF-α and Col-I protein expression levels were quantified using ELISA, this method does not provide information on protein localization or molecular weight validation. Incorporating techniques such as Western blotting or immunohistochemistry in future work would enhance the robustness of the findings by confirming protein expression patterns and tissue distribution.

Acknowledgement
None.
Financial support
None.
Conflicts of interest statement
The authors have no financial or personal interests that could be perceived as influencing the content of this work.
Author contributions
Conceptualization: ESS, MFA, and SAI; *Data curation*: MFA, SAI, AAH and MES; *Formal analysis:* MFA, SAI, AAH, and MES; *Methodology:* ESS, MFA, AH and MES; *Writing – original draft:* RMK, ESS and SAE; *Writing – review & editing:* WZ. All authors read and approved the final manuscript.
Ethics approval and consent to participate
This study was approved by the National Research Centre's Medical Research Ethics Committee in Giza, Egypt (0980223).
Consent for publication
Not applicable.
Availability of data
Data will be made available upon request from the corresponding author.

References

1. Manzuoerh R, Farahpour MR, Oryan A, Sonboli A. Effectiveness of topical administration of Anethum graveolens essential oil on MRSA-infected wounds. *Biomed Pharmacother.* 2019;109:1650-1658. doi: 10.1016/j.biopha.2018.10.117
2. Fakhry KR, Mohammed Hassan K. Formulation and evaluation of diphenhydramine HCL release from different semi-solid bases (cream, gel and ointment). *World J Pharm Res.* 2013;2:1306-1324.
3. Zainol NA, Ming TS, Darwis Y. Development and characterization of cinnamon leaf oil nanocream for topical application. *Indian J Pharm Sci.*

2015;77(4):422-433.
doi: 10.4103/0250-474x.164785

4. Koroleva MY, Yurtov EV. Nanoemulsions: The properties, methods of preparation and promising applications. *Russian Chem Rev.* 2012;81(1):21-43.
doi: 10.1070/rc2012v081n01abeh004219
5. Sumaiyah S. Formulation and evaluation of skin anti-aging nanocream containing canola (*Brassica napus* L.) oil. *Indones J Pharm Clin Res.* 2021;4(1):47-58.
doi: 10.32734/idjpcr.v4i1.5821
6. Hanum TI, Laila L, Sumaiyah S, Syahrina E. Macadamia nuts oil in nanocream and conventional cream as skin anti-aging: A comparative study. *Open Access Maced J Med Sci.* 2019;7(22):3917.
doi: 10.3889/oamjms.2019.533
7. Agili FA, Mohamed SF. Synthesis and characterization of a self-crosslinked organic copolymer kappa-carrageenan/polyacrylamide/cetrimide (κ-CAR/PAAm/CI) hydrogel with antimicrobial and anti-inflammatory activities for wound healing. *Chemistry.* 2023;5(4):2273-2287.
doi: 10.3390/chemistry5040152
8. Moro GG, Massat NC, Grandizoli DRP, *et al.* Effect of cetrimide 2% with and without photodynamic therapy to reduce *Streptococcus mutans* burden in dentinal carious lesions. *Lasers Med Sci.* 2021;36:1935-1940.
doi: 10.1007/s10103-021-03300-6
9. Kassab HJ, Merdaw MA, Al-Ramahi IJ, *et al.* Use of human umbilical cord serum to treat animal skin burns. *Iraqi J Pharm Sci.* 2019;28(2):165-173.
doi: 10.31351/vol28iss2pp165-173
10. Hong LW, Theyveeka Selvy A, Rajoo P, *et al. Channa striatus* effectiveness in wound-healing: A scoping review. *Int J Res Anal Rev.* 2020;7(1):300-308.
11. Musa AF, Min CJ. *Haruan Extract (Channa striatus) as an Effective Mediator in Promoting Wound Healing.* London: IntechOpen; 2021.
12. Orafidiya LO, Adesina SK, Igbeneghu OA, Akinkunmi EO, Adetogun GE, Salau AO. The effect of honey and surfactant type on the antibacterial properties of the leaf essential oil of *Ocimum gratissimum* Linn. against common wound-infecting organisms. *Int J Aromather.* 2006;16(2):57-62.
doi: 10.1016/j.ijat.2006.04.001
13. Abdulkarim MF, Abdullah GZ, Chitneni M, *et al.* Formulation and characterization of palm oil esters based nano-cream for topical delivery of piroxicam. *Int J Drug Deliv.* 2010;2(4):287-298.
14. Tou KAS, Rehman K, Ishak WMW, Zulfakar MH. Influence of omega fatty acids on skin permeation of a coenzyme Q10 nanoemulsion cream formulation: Characterization, *in silico* and *ex vivo* determination. *Drug Dev Ind Pharm.* 2019;45(9):1451-1458.
doi: 10.1080/03639045.2019.1628042
15. Zhou H, Yue Y, Liu G, *et al.* Preparation and characterization of a lecithin nanoemulsion as a topical delivery system. *Nanoscale Res Lett.* 2010;5:224-230.
doi: 10.1007/s11671-009-9469-5
16. Pereira RF, Bartolo PJ. Traditional therapies for skin wound healing. *Adv Wound Care.* 2016;5(5):208-229.
doi: 10.1089/wound.2013.0506
17. Kathe K, Kathpalia H. Film forming systems for topical and transdermal drug delivery. *Asian J Pharm Sci.* 2017;12(6):487-497.
doi: 10.1016/j.ajps.2017.07.004
18. de Almeida Borges VR, Simon A, Sena ARC, Cabral LM, de Sousa VP. Nanoemulsion containing dapsone for topical administration: A study of *in vitro* release and epidermal permeation. *Int J Nanomed.* 2013;8: 535-544.
doi: 10.2147/IJN.S39383
19. Karami Z, Khoshkam M, Hamidi M. Optimization of olive oil-based nanoemulsion preparation for intravenous drug delivery. *Drug Res.* 2019;69(5):256-264.
doi: 10.1055/a-0654-4867
20. Salama A, Mohasib RM, Shalaby ES. Neuroprotective role of *Origanum majorana* essential oil loaded in mixed surfactants based nano emulsion against lipopolysaccharide-induced Alzheimer in mice. *J Pharm Investig.* 2025;55:265-281.
doi: 10.1007/s40005-024-00696-5
21. Samadi A, Sartipi Z, Ahmad Nasrollahi S, *et al.* Efficacy assessments of tretinoin-loaded nano lipid carriers in acne vulgaris: A double blind, split-face randomized clinical study. *Arch Dermatol Res.* 2021;314(6): 553-561.
doi: 10.1007/s00403-021-02256-5
22. Ammar HO, Ghorab MM, Mostafa DM, *et al.* Development of folic acid–loaded nanostructured lipid carriers for topical delivery: Preparation, characterisation and *ex vivo* investigation. *J Microencapsul.* 2020;37(5):366-383.
doi: 10.1080/02652048.2020.1761904
23. Elmotasem H, Salama AA, Shalaby ES. Hyaluronate functionalized Span-Labrasol nanovesicular transdermal therapeutic system of ferulic acid targeting diabetic nephropathy. *Int J Biol Macromol.* 2024; 279:135292.
doi: 10.1016/j.ijbiomac.2024.135292
24. Shalaby ES, Abdelhameed MF, Ismail SA, Ahmed YH, Aboutaleb S. Innovative Indian propolis loaded carnauba wax based lipid structured nanocarriers: Preparation, characterization and *in vitro/in vivo* antifungal activities. *BioNanoScience.* 2024;14:1726-1743.
doi: 10.1007/s12668-024-01361-9
25. Sathe MA, Rajput SJ. Exploration of various classical and chemometric assisted uv spectrophotometric methods for estimation of chlorhexidine gluconate and cetrimide in bulk and its formulation. *Am J Pharm Res.* 2017;7(8):414-425.
26. Asfour MH, Mohsen AM. Formulation and evaluation of pH-sensitive rutin nanospheres against colon carcinoma using HCT-116 cell line. *J Adv Res.* 2018;9:17-26.
doi: 10.1016/j.jare.2017.10.003
27. Elhabak M, Ibrahim S, Abouelatta SM. Topical delivery of l-ascorbic acid spanlastics for stability enhancement and treatment of UVB induced damaged skin. *Drug Deliv.* 2021;28(1):445-453.
doi: 10.1080/10717544.2021.1886377
28. Beaulac C, Clement-Major S, Hawari J, Lagace J. *In vitro* kinetics of drug release and pulmonary retention of microencapsulated antibiotic in liposomal formulations in relation to the lipid composition. *J Microencapsul.* 1997;14(3):335-348.
doi: 10.3109/02652049709051137
29. Shamma RN, Sayed S, Sabry NA, El-Samanoudy SI. Enhanced skin targeting of retinoic acid spanlastics: *In vitro* characterization and clinical evaluation in acne patients. *J Liposome Res.* 2019;29(3):283-290.
doi: 10.1080/08982104.2018.1552706
30. Balouiri M, Sadiki M, Ibnsouda SK. Methods for *in vitro* evaluating antimicrobial activity: A review. *J Pharm Anal.* 2016;6(2):71-79.
doi: 10.1016/j.jpha.2015.11.005
31. Sharpe JR, Martin Y. Strategies demonstrating efficacy in reducing wound contraction *in vivo. Adv Wound Care.* 2013;2(4):167-175.
doi: 10.1089/wound.2012.0378
32. Shaheen TI, Abdelhameed MF, Zaghloul S, Montaser A. *In vivo* assessment of the durable, green and *in situ* bio-functional cotton fabrics based carboxymethyl chitosan nanohybrid for wound healing application. *Int J Biol Macromol.* 2022;209:485-497.
doi: 10.1016/j.ijbiomac.2022.04.027
33. Afifi N, Ramadan A, El-Eraky W, Salama A, El-Fadaly A, Hassan A. Quercetin protects against thioacetamide induced hepatotoxicity in rats through decreased oxidative stress biomarkers, the inflammatory cytokines;(TNF-α),(NF-κ B) and DNA fragmentation. *Der Pharma Chem.* 2016;8(9):48-55.
34. Khalil RM, Abdelhameed MF, Taleb SA, El-Saied MA, Shalaby ES. Preparation and characterization of Esculetin loaded nanostructured lipid carriers gels for topical treatment of UV-induced psoriasis. *Pharm Dev Technol.* 2024;29(8):886-898.
doi: 10.1080/10837450.2024.2407854
35. Gal P, Kilik R, Mokry M, *et al.* Simple method of open skin wound healing model in corticosteroid-treated and diabetic rats: Standardization of semi-quantitative and quantitative histological assessments. *Vet Med.* 2008;53(12):652-659.
36. Kotta S, Khan AW, Ansari SH, Sharma RK, Ali J. Formulation of nanoemulsion: A comparison between phase inversion composition method and high-pressure homogenization method. *Drug Deliv.* 2015;22(4):455-466.
doi: 10.3109/10717544.2013.866992

37. Mahdi ES, Noor AM, Sakeena MH, Abdullah GZ, Abdulkarim MF, Sattar MA. Formulation and *in vitro* release evaluation of newly synthesized palm kernel oil esters-based nanoemulsion delivery system for 30% ethanolic dried extract derived from local *Phyllanthus urinaria* for skin antiaging. *Int J Nanomed.* 2011;6:2499-2512. doi: 10.2147/IJN.S22337
38. Akhtar J, Siddiqui HH, Fareed S, Badruddeen, Khalid M, Aqil M. Nanoemulsion: For improved oral delivery of repaglinide. *Drug Deliv.* 2016;23(6):2026-2034. doi: 10.3109/10717544.2015.1077290
39. Chinnaiyan SK, Pandiyan R, Natesan S, Chindam S, Gouti AK, Sugumaran A. Fabrication of basil oil Nanoemulsion loaded gellan gum hydrogel-evaluation of its antibacterial and anti-biofilm potential. *J Drug Deliv Sci Technol.* 2022;68:103129. doi: 10.1016/j.jddst.2022.103129
40. Morais JM, Burgess DJ. *In vitro* release testing methods for vitamin E nanoemulsions. *Int J Pharm.* 2014;475(1-2):393-400. doi: 10.1016/j.ijpharm.2014.08.063
41. Kanekar S, Rao SS, Yuvarajan S, Surya S, Rekha PD. Linalool-encapsulated alginate microspheres as anti-virulence target against wound infections using *in vitro* and *in vivo* models. *J Drug Deliv Sci Technol.* 2022;77:103848. doi: 10.1016/j.jddst.2022.103848
42. Prakash A, Vadivel V. Citral and linalool nanoemulsions: Impact of synergism and ripening inhibitors on the stability and antibacterial activity against *Listeria monocytogenes*. *J Food Sci Technol.* 2020;57(4):1495-1504. doi: 10.1007/s13197-019-04185-8
43. Heydari Gharehcheshmeh M, Arianfar A, Mahdian E, Naji-Tabasi S. Production and evaluation of sweet almond and sesame oil nanoemulsion and their effects on physico-chemical, rheological and microbial characteristics of enriched yogurt. *J Food Measur Character.* 2021;15(2):1270-1280. doi: 10.1007/s11694-020-00711-x
44. Sallam KI, Abd-Elghany SM, Imre K, *et al.* Ensuring safety and improving keeping quality of meatballs by addition of sesame oil and sesamol as natural antimicrobial and antioxidant agents. *Food Microbiol.* 2021;99:103834. doi: 10.1016/j.fm.2021.103834
45. Bodmeier R, Wang J, Bhagwatwar H. Process and formulation variables in the preparation of wax microparticles by a melt dispersion technique. II. W/O/W multiple emulsion technique for water-soluble drugs. *J Microencapsul.* 1992;9(1):99-107. doi: 10.3109/02652049209021226
46. Viswanathan NB, Thomas P, Pandit J, Kulkarni M. Preparation of non-porous microspheres with high entrapment efficiency of proteins by a (water-in-oil)-in-oil emulsion technique. *J Control Release.* 1999;58(1):9-20. doi: 10.1016/S0168-3659(98)00140-0
47. Wei YS, Niu ZC, Wang FQ, Feng K, Zong MH, Wu H. A novel pickering emulsion system as the carrier of tocopheryl acetate for its application in cosmetics. *J Mater Sci Eng C.* 2020;109:110503. doi: 10.1016/j.msec.2019.110503
48. Liao Y, Zhong L, Liu L, *et al.* Comparison of surfactants at solubilizing, forming and stabilizing nanoemulsion of hesperidin. *J Food Eng.* 2020;281:110000. doi: 10.1016/j.jfoodeng.2020.110000
49. Hidajat MJ, Jo W, Kim H, Noh J. Effective droplet size reduction and excellent stability of limonene nanoemulsion formed by high-pressure homogenizer. *Colloids Interfaces.* 2020;4(1):5. doi: 10.3390/colloids4010005
50. Zhao C, Wei L, Yin B, *et al.* Encapsulation of lycopene within oil-in-water nanoemulsions using lactoferrin: Impact of carrier oils on physicochemical stability and bioaccessibility. *Int J Biol Macromol.* 2020;153:912-920. doi: 10.1016/j.ijbiomac.2020.03.063
51. Şenyiğit T, Sonvico F, Barbieri S, Özer Ö, Santi P, Colombo P. Lecithin/chitosan nanoparticles of clobetasol-17-propionate capable of accumulation in pig skin. *J Control Release.* 2010;142(3):368-373. doi: 10.1016/j.jconrel.2009.11.013
52. Chu CC, Hasan ZABA, Chua SK, Nyam KL. Formulation and characterization of novel nanostructured lipid carriers with photoprotective properties made from Carnauba Wax, Beeswax, pumpkin seed oil, and UV filters. *J Am Oil Chem Soc.* 2020;97(5):531-542. doi: 10.1002/aocs.12340
53. Shafiq S, Shakeel F, Talegaonkar S, Ahmad FJ, Khar RK, Ali M. Development and bioavailability assessment of ramipril nanoemulsion formulation. *Eur J Pharm Biopharm.* 2007;66(2):227-243. doi: 10.1016/j.ejpb.2006.10.014
54. Bali V, Ali M, Ali J. Study of surfactant combinations and development of a novel nanoemulsion for minimising variations in bioavailability of ezetimibe. *Colloids Surf B Biointerfaces.* 2010;76(2):410-420. doi: 10.1016/j.colsurfb.2009.11.021
55. Cardoso SA, Barradas TN. Developing formulations for drug follicular targeting: Nanoemulsions loaded with minoxidil and clove oil. *J Drug Deliv Sci Technol.* 2020;59:101908. doi: 10.1016/j.jddst.2020.101908
56. Baba Shekh AO, Abdul Wahab R, Yahya NA. Formulation of roselle extract water-in-oil nanoemulsion for controlled pulmonary delivery. *J Dispersion Sci Technol.* 2022;40:1-12. doi: 10.1080/01932691.2022.2046044
57. Lv G, Wang F, Cai W, Zhang X. Characterization of the addition of lipophilic Span 80 to the hydrophilic Tween 80-stabilized emulsions. *Colloids Surf A Physicochem Eng Aspects.* 2014;447:8-13. doi: 10.1016/j.colsurfa.2014.01.066
58. Đorđević SM, Radulović TS, Cekić ND, *et al.* Experimental design in formulation of diazepam nanoemulsions: Physicochemical and pharmacokinetic performances. *J Pharm Sci.* 2013;102(11):4159-4172. doi: 10.1002/jps.23734
59. Wahab A, Khan GM, Akhlaq M, *et al.* Pre-formulation investigation and *in vitro* evaluation of directly compressed ibuprofen-ethocel oral controlled release matrix tablets: A kinetic approach. *Afr J Pharm Pharmacol.* 2011;5(19):2118-2127.
60. Basha M, Abd El-Alim SH, Shamma RN, Awad GE. Design and optimization of surfactant-based nanovesicles for ocular delivery of Clotrimazole. *J Liposome Res.* 2013;23(3):203-210. doi: 10.3109/08982104.2013.788025
61. Cai S, Wang L, Cui X, *et al.* Rhein-loaded chitosan nanoparticles for treatment of MRSA-infected wound. *Int J Biol Macromol.* 2024;279:135360. doi: 10.1016/j.ijbiomac.2024.135360
62. Mirzamani SS, Farahpour MR, Tabatabaei ZG. Enhanced MRSA-infected wound healing using tannic acid cross-linked carboxymethyl chitosan/polyglutamic acid hydrogel for carbazole Delivery. *Colloids Surf B Biointerfaces.* 2025;249:114490. doi: 10.1016/j.colsurfb.2024.114490
63. Farasati Far B, Naimi-Jamal MR, Sedaghat M, Hoseini A, Mohammadi N, Bodaghi M. Combinational system of lipid-based nanocarriers and biodegradable polymers for wound healing: An updated review. *J Funct Biomater.* 2023;14(2):115. doi: 10.3390/jfb14020115
64. Abraham NG, Kappas A. Pharmacological and clinical aspects of heme oxygenase. *Pharmacol Rev.* 2008;60(1):79-127. doi: 10.1124/pr.107.07104
65. Hussein RA, Salama AA, El Naggar ME, Ali GH. Medicinal impact of microalgae collected from high rate algal ponds; phytochemical and pharmacological studies of microalgae and its application in medicated bandages. *Biocatal Agric Biotechnol.* 2019;20:101237. doi: 10.1016/j.bcab.2019.101237
66. Abdel-Hakeem MA, Mongy S, Hassan B, Tantawi OI, Badawy I. Curcumin loaded chitosan-protamine nanoparticles revealed antitumor activity via suppression of NF-κB, proinflammatory cytokines and Bcl-2 gene expression in the breast cancer cells. *J Pharm Sci.* 2021;110(9):3298-3305. doi: 10.1016/j.xphs.2021.06.004
67. Kisling A, Lust RM, Katwa LC. What is the role of peptide fragments of collagen I and IV in health and disease? *Life Sci.* 2019;228:30-34. doi: 10.1016/j.lfs.2019.04.042

68. Mathew-Steiner SS, Roy S, Sen CK. Collagen in wound healing. *Bioengineering*. 2021;8(5):63. doi: 10.3390/bioengineering8050063
69. Rai NK, Tripathi K, Sharma D, Shukla VK. Apoptosis: A basic physiologic process in wound healing. *Int J Low Extrem Wounds*. 2005;4(3): 138-144. doi: 10.1177/1534734605280018
70. Moalla Rekik D, Ben Khedir S, Ksouda Moalla K, Kammoun NG, Rebai T, Sahnoun Z. Evaluation of wound healing properties of grape seed, sesame, and fenugreek oils. *Evid Based Complement Alternat Med*. 2016;2016(1):7965689. doi: 10.1155/2016/7965689
71. Sharif MR, Alizarger J, Sharif A. Evaluation of the wound healing activity of sesame oil extract in rats. *World J Med Sci*. 2013;9(2):74-78.

Received: May 21, 2025
Revised: July 20, 2025
Accepted: July 21, 2025
Available online: August 21, 2025